Phase correction in Gabor deconvolution

Carlos A. Montaña and Gary F. Margrave

ABSTRACT

The constant-Q theory for anelastic attenuation is reviewed, particularly the aspects related with the determination of the phase of the attenuated signal and the potential error introduced by the discrete implementation of the Hilbert transform. Synthetic data are used to test the phase correction in the Gabor deconvolution and to compare it with the results obtained by inverse-Q filter methods. The maximum coefficient of a local crosscorrelation and its lag are used as attributes to estimate the similarity between the expected and the real output. Particularly the crosscorrelation lag is used as indicator of the phase correction. The uncertainty associated with the estimation of Q is included as variable by applying inverse-Q filter with a different Q from the one used to model the attenuated trace.

INTRODUCTION

Different methods have been developed and are in use to compensate for anelastic attenuation in seismic data. Time-variant spectral whitening and inverse-Q filter are among the most widely known and used. More recently the Gabor deconvolution method has emerged as a powerful tool to deal with this challenging problem.

Anelastic attenuation is just one of the mechanisms by which seismic waves travelling through an anelastic medium are attenuated. Other attenuation mechanisms are geometric spreading, absorption, transmission losses, S- and P-mode conversion, scattering, and refraction at critical angles. Each of these mechanisms requires a separate treatment to compensate for their nonstationary effects on the seismic signal. In general, the optimal correction of attenuation requires the combination of different methods; each one specialized in a specific attenuation mechanism.

As a wave travels through an anelastic medium, internal friction between the perturbed particles causes that part of the transported mechanical energy be transformed into heat. The dimensionless parameter Q, called the quality factor or attenuation parameter, is the most common macroscopic variable used to quantify anelastic attenuation effects and is defined as the ratio between the total and the lost energy per wave cycle. Different physical mathematical models, based on experimental results, have been proposed to represent anelastic attenuation. In the range of seismic frequencies used in data processing, both in exploration and earthquake seismology, the constant Q or frequency-independent Q model have turned out to be a simple and at the same time sufficiently accurate model to represent anelastic attenuation.

The constant-Q model (e.g., Aki and Richards, 2001) is the underlying theoretical support for both Gabor deconvolution and inverse-Q filter methods. Its basic assumptions are linearity, frequency-independent Q and velocity dispersion. A theoretical model for an attenuated trace can be derived from the constant-Q model which is useful for analyzing the effects of anelastic attenuation and for searching different methods of correcting them. These effects on the signal can be summarized in amplitude decaying,

due to energy absorption, waveshape modification, due to stronger absorption of higher frequencies, and phase delaying, due to dispersion.

The Gabor deconvolution has been tested in real data and compared with conventional surface-consistent Wiener deconvolution followed by time-variant spectral whitening (Margrave et al., 2004). The resolution of data processed with Gabor deconvolution has been found better than the resulting from conventional processing. In the last mentioned paper there is also a comparison of the amplitude recovery from Gabor deconvolution with the obtained from conventional processing. However, very little has been done to evaluate the performance of Gabor deconvolution in compensating for the phase distortion. The purpose of this paper is to carry out a first assessment of this issue, by evaluating the phase recovery on Gabor-deconvolved synthetic data and comparing it with the results obtained from inverse-Q filtering methods. A review and comparison of the different existing methods for applying a Q filter can be found in Montaña and Margrave (2004).

THEORY

A nonstationary model for the attenuated trace

The constant-Q theory (Kjartansson, 1979) establishes a model for the attenuated trace based on two main assumptions: frequency independence of Q and linearity. Although field measurements of attenuation show a slightly variation of Q with frequency, the assumption of frequency- independent Q allows to build a simple and powerful model for anelastic attenuation, consistent, within the range of uncertainty associated with field measurements, with experimental data. The assumption of linearity is broadly confirmed by observations, except for strong attenuation (Q<10) and for wave propagation very near the source.

A fundamental result from the theory of linear filters is that a linear filter is completely characterized by its impulse response. For this reason, the attenuation effects on a travelling wave can be determined by examining the attenuating medium impulse response. A first basic result of assuming Q constant and linearity is that the impulse response $p(x,t)$ is given by the expression

$$p(x,t)=\frac{1}{\pi}\left[\frac{\frac{x}{2\upsilon Q}}{\left(\frac{x}{2\upsilon Q}\right)^2+\left(\frac{x}{\upsilon}-t\right)^2}\right], \qquad (1)$$

where x is the travel distance, Q is the attenuation parameter, υ is the frequency-independent velocity, and t is the traveltime (Aki and Richards, 2001). Figure 1 (blue line) shows the plotting of Equation (1) in which the exponential decay of the amplitude and the progressive broadening of the pulse are observed. The amplitude decay is a direct consequence of the transference of energy to the medium. The pulse broadening is generated by the stronger absorption of energy from the plane-wave components with higher frequencies. Both effects are consistent with experimental observations. Other characteristics of this impulse response are not consistent with observations: its symmetry

and its noncausality. To reconcile the model with the observations regarding the pulse shape, velocity dispersion must be considered.

In Aki and Richards' (2001) approach, dispersion arises as a consequence of imposing causality as a constraint, i.e. $p(x,t)=0$ for $t < x/v_\infty$, where v_∞ is the group velocity, which corresponds to the common sense expectation that no response can be detected before the arrival of the travelling wave. Consideration of causality forces the attenuation function, the velocity and the frequency to be related through

$$\frac{\omega}{v(\omega)} = \frac{\omega}{v_\infty} + \mathrm{H}[\alpha(\omega)], \tag{2}$$

where

$$\alpha(\omega) = \frac{\omega}{2v(\omega)Q}, \tag{3}$$

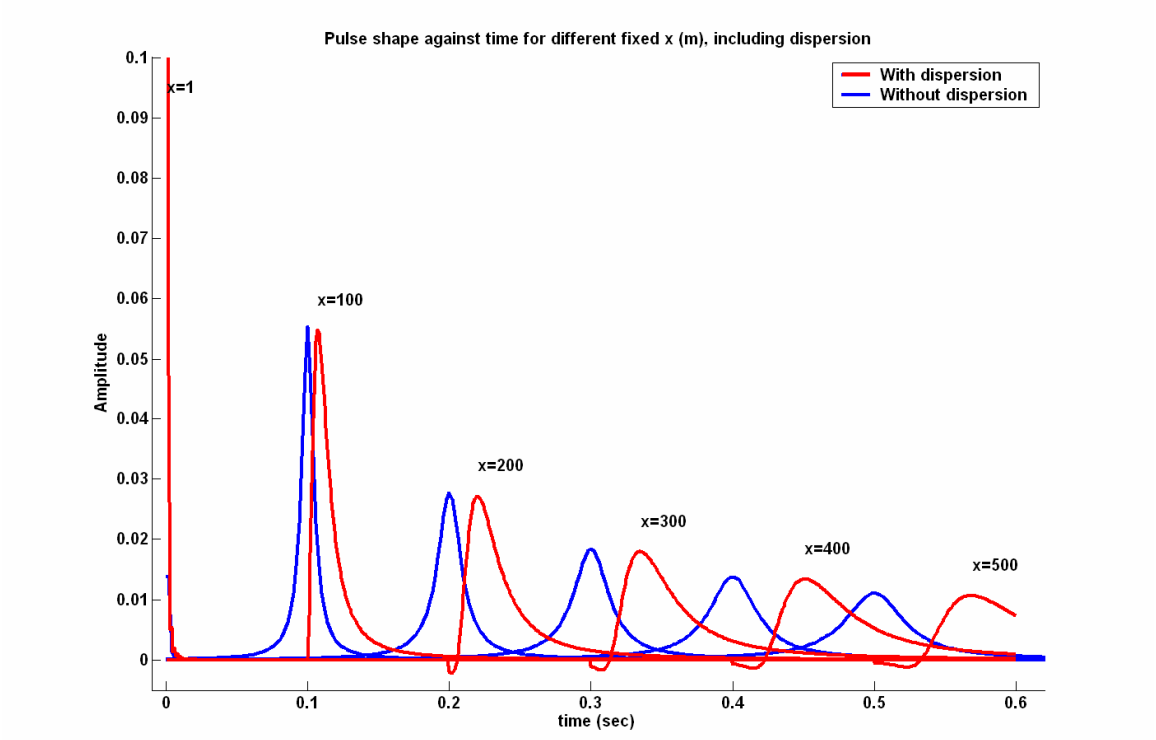

FIG. 1. A pulse source is modified when travelling through an anelastic medium. Its amplitude decaying exponentially, the pulse broadens and a phase delay appears if dispersion is considered. The blue pulse corresponds to plotting Equation (1) for different fixed-x travel distances and does not consider dispersion. When dispersion is included the resulting pulse is the red one.

is the attenuation function, and $\mathrm{H}[\alpha(t)]$ is the Hilbert transform of the attenuation function. The appearance of the Hilbert transform at this point is completely expected

because, for causal functions, the amplitude spectrum is completely determined by its phase spectrum and vice-versa through their Hilbert transforms.

The combination of Equations (2) and (3) takes to

$$2Q\alpha(\omega) = \frac{\omega}{v_\infty} + \mathrm{H}[\alpha(\omega)], \tag{4}$$

which can not be satisfied for constant-Q. By considering a generally frequency-dependent Q, but effectively constant over the seismic frequency range, the ratio of two velocities at two different seismic frequencies is established as

$$\frac{v(\omega_1)}{v(\omega_2)} = 1 + \frac{1}{\pi Q}\log\left(\frac{\omega_1}{\omega_2}\right). \tag{5}$$

An additional consequence of establishing causality as a constraint is to confer the minimum-phase character to the impulse response *p(x,t)*. Dispersion, causality and minimum-phase are essential concepts for the attenuation constant-*Q* theory which are intimately linked with each other.

Other dispersion relations are proposed in the literature; for example Kjartansson (1979) uses

$$v(\omega) = v(\omega_0)\left|\frac{\omega}{\omega_0}\right|^{\frac{1}{\pi Q}}. \tag{6}$$

The consequence of introducing dispersion into the constant-*Q* theory is that the attenuating medium impulse response in the frequency domain is given by

$$B(\omega) = \exp\left[-\frac{\omega x}{2v_\infty Q}\right]\exp\left[\frac{-i\omega x}{v(\omega)}\right]. \tag{7}$$

A source pulse travelling through an anelastic medium, modelled from Equation (7), is shown in Figure 1 (red line). Once the impulse response is determined, a model for the attenuated trace (for the case of a pulse source) follows logically as a nonstationary convolution between the reflectivity and the impulse response, according to the theory of nonstationary linear filters (Margrave, 1998). The inverse Fourier transform of Equation (7) nonstationaryly convolved with the reflectivity wavelet, yields the attenuated seismic trace for an impulsive source (Margrave et al., 2002),

$$s_Q(t) = \frac{1}{2\pi}\int_{-\infty}^{\infty}\int_{-\infty}^{\infty}\alpha_Q(\omega,\tau)r(\tau)e^{i\omega(t-\tau)}d\tau d\omega, \tag{8}$$

where

$$\alpha_Q(\omega,\tau) = \exp\left(-\omega\tau/2Q + iH(\omega\tau/2Q)\right), \tag{9}$$

is the exponential attenuation function and $\tau = x/v_\infty$. By a stationary convolution of Equation (8) with an arbitrary source wavelet *w(t)*, a general nonstationary trace can be generated,

$$\hat{s}(\omega) = \frac{1}{2\pi}\hat{w}(\omega)\int_{-\infty}^{\infty}\alpha_Q(\omega,\tau)r(\tau)e^{i\omega(t-\tau)}d\tau. \tag{10}$$

Equation (10) shows the result of the stationary deconvolution in the Fourier domain. The 'hat' symbol indicates Fourier transform.

Phase delay in modelling an attenuated trace

If Equation (10) is used to model an attenuated trace, an important aspect in the modeling is how to compute the phase delay in the exponential attenuation function, Equation (9). This phase delay is determined by the Hilbert transform of a function of frequency and can be found either analytically, by using Equation (2), or digitally, by using the definition of the Hilbert transform,

$$H\left(\frac{\omega\tau}{2Q}\right) = \frac{1}{\pi}\int_{-\infty}^{\infty}\frac{\frac{\omega'\tau}{2Q}}{\omega'-\omega}d\omega'. \tag{11}$$

To compute the phase delay from the definition given to the Hilbert transform in Equation (11), a corresponding finite discrete definition must be used,

$$H\left(\frac{\omega\tau}{2Q}\right) = \frac{1}{\pi}\sum_{n=-N}^{N}\frac{\frac{\omega_n\tau}{2Q}}{\omega_n-\omega}\Delta\omega. \tag{12}$$

The digital method to compute the phase, using Equation (12), has the disadvantage of substituting the infinite limits in the definition of the Hilbert transform with finite limits determined by the sample rate. An error in the phase delay is introduced by using this approach.

The difference in phase delay between the two methods is estimated by computing a windowed crosscorrelation between two pieces of trace within the same time interval. The maximum coefficient of the local crosscorrelation (MAXCORR) gives an estimation of the similarity between the two segments and its lag can be considered as an indicator of their phase difference.

This comparison method is applied to two traces, Figure 3, modelled by the analytic method, the blue one, and by the digital method, the cyan one. The rightmost plot in Figure 3, corresponds to the maximum crosscorrelation lag between the analytic and the digital modelled trace. A linear, growing with time, trend can be observed in the lag, which almost reaches the 4 ms. In Figure 4, three events at different times are enlarged to observe with better detail the phase difference.

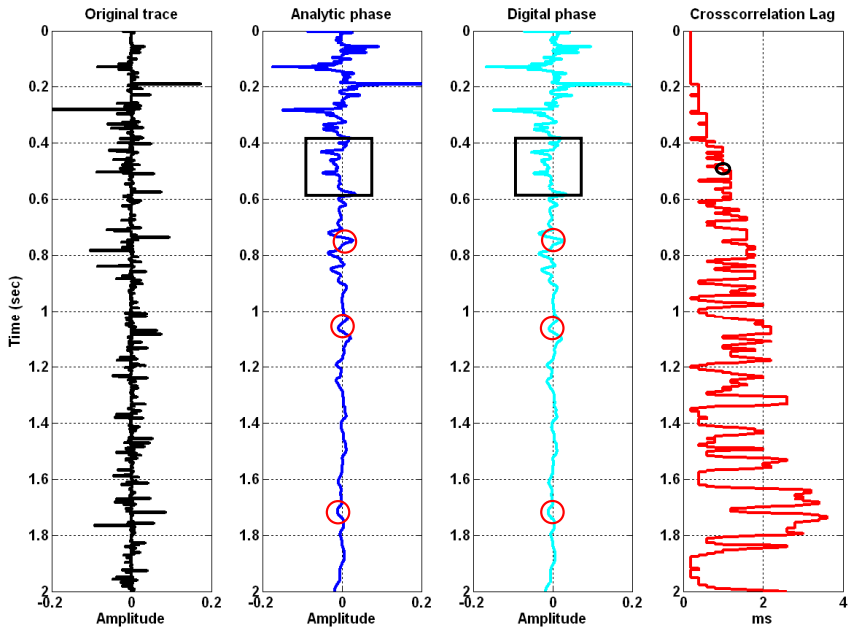

FIG. 2. A random reflectivity series (leftmost) is used to generate two attenuated traces. The Hilbert transform for the phase of the attenuation function is computed in the analytic case (second from the left) using Equation (2). In the digital case, the Hilbert transform is estimated by the discrete Equation (12). The lag of the maximum crosscorrelation coefficient (rightmost) between two corresponding pieces of traces is used as indicator of the phase difference between the two attenuated traces. To find the circled point value, the shown windowed pieces of the analytical and digital traces were used. In the example shown, the digital trace has greater phase delay than the analytic one. A *Q* value of 50 was used.

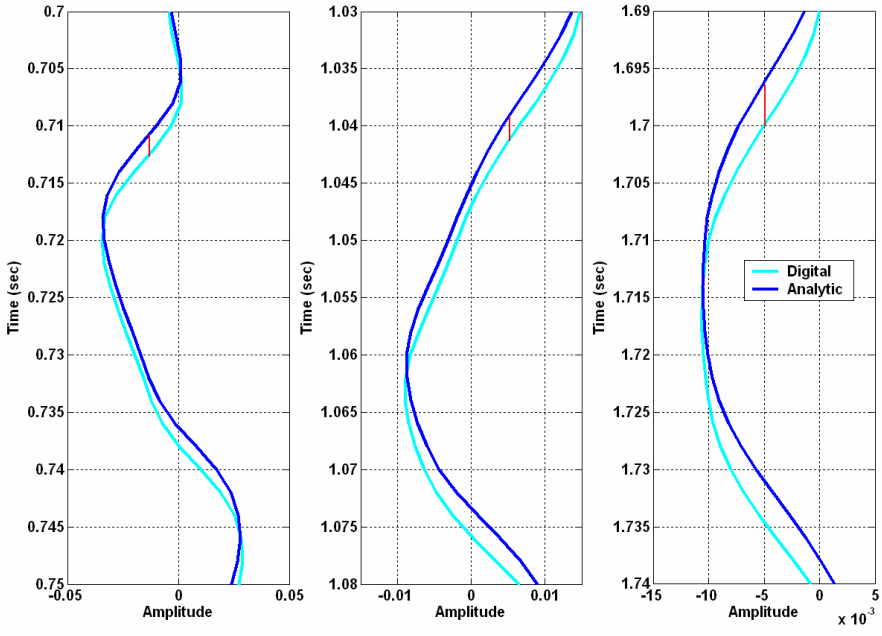

FIG. 3. Enlargement of the circled events in the previous Figure. The vertical scale in the three plots is the same but the horizontal scale has been modified in each plot to ease the observation of the growing phase delay.

It can be seen that a growing phase difference exists between the two modelled traces. It is worthwhile to point out that for the latest event, the phase difference is almost 4 ms, from which a confirmation of the reliability of the crosscorrelation lag as an estimate of the phase delay is reached. A Q value of 50 was used in this test. The MAXCORR and its lag will be used henceforth as attributes to measure the similarity between the expected output and the real output from the Gabor deconvolution and the inverse-Q filter methods. In Figure 4, the resulting crosscorrelation lag is shown for different values of Q. The phase lag tends to increase when Q decreases.

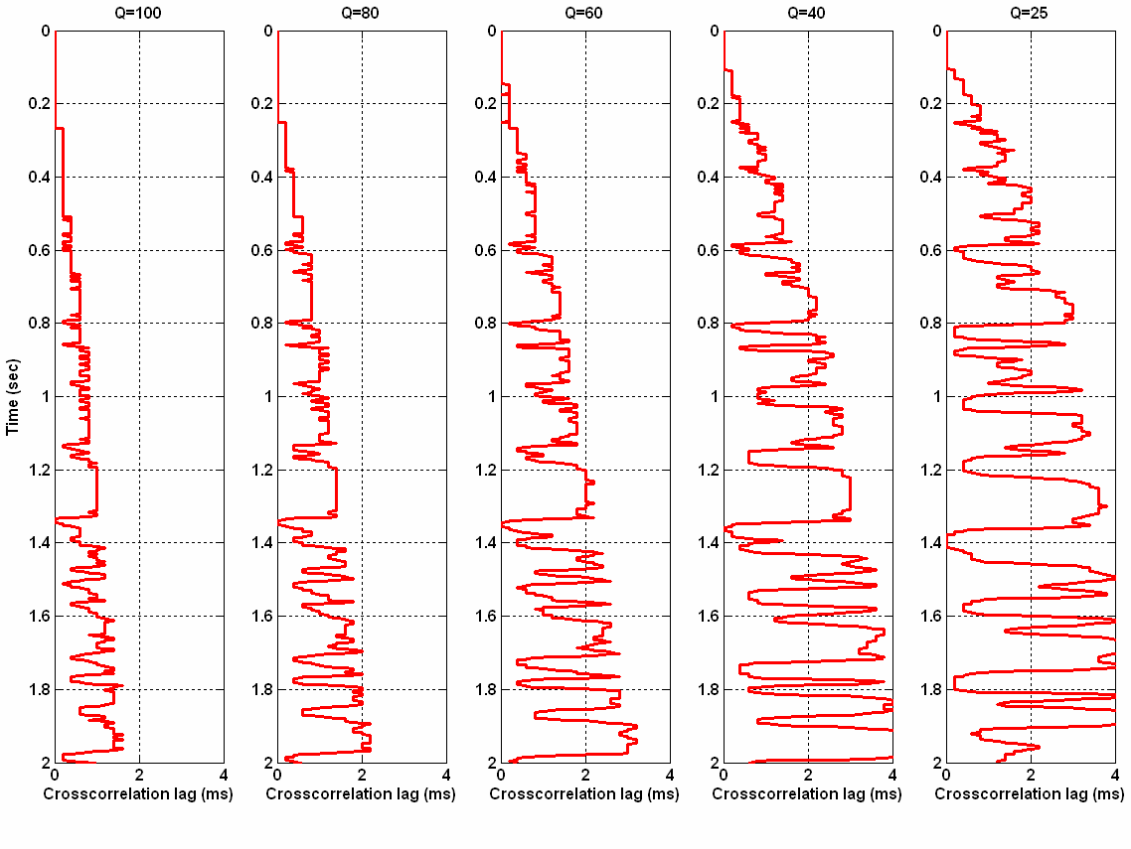

FIG. 4. The lag of the maximum coefficient of the crosscorrelation between the analytic and the digital attenuated traces for different Q values. An approximately linear trend, growing with time, can be observed for each Q value. When Q decreases the lag tends to increase. For Q values less than 25 and long times, the traces are so attenuated that the correlation lag is not reliable as a phase-delay indicator anymore.

The Gabor transform and the spectrogram

The Fourier transform of a signal gives the relative weights of the various monochromatic components that make up the signal. It tells which frequencies exist and their strengths. However it does not tell where those frequencies are localized in the time domain. In contrast, time-frequency representations are functions of time and frequency which display the frequency content of signals for different times. Among the more

widely used time-frequency representations in signal processing are the Gabor transform and the spectrogram.

One way of obtaining the time-dependence frequency content of a signal *s(t)*, is to take its Fourier transform over an interval around a point $t=\tau$, where τ is a variable parameter. This is the Gabor transform and may be defined as follows (e.g., Mertins, 1999):

$$V_g s(\tau, f) = \int_{-\infty}^{\infty} s(t) g(t-\tau) e^{-2\pi i f t} dt \ , \tag{13}$$

where $g(t)$ is the Gabor analysis window, f is the frequency, and τ is the location of the window centre.

The inverse Gabor transform is defined as

$$s(t) = \int_{-\infty}^{\infty}\int_{-\infty}^{\infty} V_g s(\tau, f) \gamma(t-\tau) e^{2\pi i f t} df d\tau \ , \tag{14}$$

where $\gamma(t)$ is the Gabor synthesis window. $g(t)$ and $\gamma(t)$ must satisfy the condition

$$\int_{-\infty}^{\infty} g(t)\gamma(t) dt = 1 \ . \tag{15}$$

Margrave et al. (2002) developed a particular implementation, appropriate for discrete sampled bandlimited signals, based on the concept of partition of unity. A partition of unity is a collection of real-valued windows chosen in such way that they sum to 1 everywhere. A highly efficient Discrete Gabor Transform algorithm can be obtained by the implementation of a partition of unity based on Lamoureux windows (Grossman et al., 2002).

The absolute squared of the Gabor transform is known as the spectrogram (e.g. Cohen, 1995):

$$P_{SP}(\tau, f) = \left| V_g s(\tau, f) \right|^2 = \left| \int_{-\infty}^{\infty} s(t) g(t-\tau) e^{-2\pi i f t} dt \right|^2 \ . \tag{16}$$

The spectrogram $P_{SP}(\tau, f)$ can be interpreted as an indicator of the signal energy at the time and frequency point (τ,*f*). Both in the spectrogram and in the Gabor transform, resolution in time and frequency are governed by the uncertainty principle. Improving time localization by using a shorter window, results in a broadening of the local spectrum and consequently frequency localization deteriorates. The reverse happens when lengthening the time window: frequency resolution is improved at the cost of time resolution. Figure 5 (right) shows the absolute value of the Gabor transform of a nonstationary signal (left).

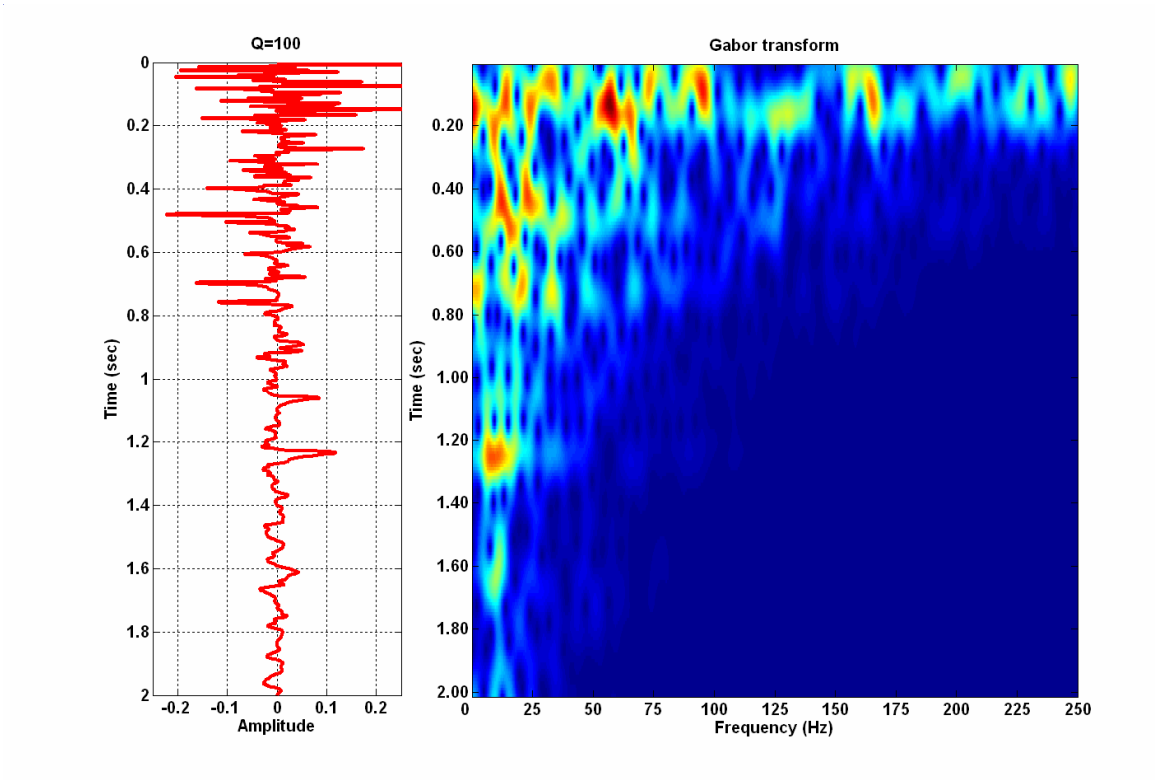

FIG. 5. Gabor transform (right) of an attenuated signal (left). The frequency content of the signal can be directly observed on the Gabor transform.

The Gabor deconvolution

Margrave and Lamoureux (2002) have proposed an asymptotic factorization of the nonstationary trace model of Equation (10), based on the Gabor transform,

$$V_g s(\tau, f) \approx \hat{w}(f)\alpha_Q(\tau, f)V_g r(\tau, f), \qquad (17)$$

which states that the Gabor transform of the seismic trace, $V_g s(\tau, f)$, is approximately equal to the product of the Fourier transform of the source wavelet, $\hat{w}(f)$, the time-frequency attenuation function, $\alpha_Q(\tau, f)$, and the Gabor transform of the reflectivity $V_g r(\tau, f)$. The Gabor deconvolution is a non-stationary extension of the Wiener deconvolution method in the frequency domain and implies a minimum-phase source wavelet and white reflectivity series. The method assumes that $|V_g r(\tau, f)|$ is a rapidly varying function in both variables τ and f, $|\hat{w}(f)|$ is smoothly varying in f, and $\alpha_Q(\tau, f)$ is an exponentially decaying function in both variables τ and f, and constant over hyperbolic families of τf=*constant.* An approximation $|\sigma(\tau, f)|$ of $|\hat{w}(f)|\,|\alpha_Q(\tau, f)|$ is obtained by applying a smoothing operation to $|V_g s(\tau, f)|$. Different kinds of smoothing are possible; Iliescu and Margrave (2002) use 2-D boxcar smoothing and hyperbolic smoothing, along curves of τf=*constant.* Grossman et al. (2002) use a different method to

estimate $|\hat{w}(f)|$ and $|\alpha_Q(\tau, f)|$ based on a least square fitting of Equation (17). As $\sigma(\tau, f)$ represents the attenuated source wavelet, its minimum-phase function is estimated from $|\sigma(\tau, f)|$ using the Hilbert transform:

$$\varphi(\tau, f) = \int_{-\infty}^{\infty} \frac{\ln|\sigma(\tau, f')|}{f - f'} df' . \qquad (18).$$

Finally the Gabor spectrum of the reflectivity is estimated in the Gabor domain as:

$$V_g r(\tau, f)_{est} = \frac{V_g(\tau, f)}{\sigma(\tau, f)} . \qquad (19)$$

Gabor vs. *Q* filter phase correction

By using the Hilbert transform to compute the phase spectrum of the attenuated source wavelet, the problem of substituting the infinite limits of the Hilbert transform integral by finite limits arises again. The difference is that now there is no analytical expression to find the accurate phase function and only a digital estimation is at hand. It is very important to know the length of the phase delay remaining after Gabor deconvolution as a result of the error introduced in the computation of the Hilbert transform.

By using synthetic seismic data, an assessment of the phase delay remaining after applying Gabor deconvolution and a comparison with the results obtained by using *Q* filtering can be carried out. The phase correction performed by the *Q* filter methods is highly accurate when the exact value of *Q* is available (e.g., Montana and Margrave, 2004). However, in practice, *Q* is estimated from surface seismic data, VSP data, or derived from other properties, for example as 1% of the velocity. Among the three methods for estimating Q, the VSP is the most accurate, but unfortunately, given that the VSP data requires a borehole, only on few occasions is this kind of data available. The estimation of *Q* from the other mentioned methods involves uncertainty grades as high as 100%.

Given the uncertainty surrounding Q, it is reasonable to evaluate the performance of the two kinds of methods by assuming an error in *Q* estimation. A random reflectivity series is used as a reference trace, without convolving it with a source wavelet to avoid mixing the error from the *Q* filters with the error from the stationary deconvolution necessary to remove the source signature. An attenuated trace is modelled by nonstationarily convolving the reference stationary trace with the nonstationary impulse response corresponding to a value Q_1. This attenuated trace is then subject to Gabor deconvolution, on the one hand, and inverse-*Q* filter (using a value Q_2), on the other, and the results compared. For weak attenuation (Q>100), the Hale inverse-*Q* filter method is used due to its unmatched accuracy. For strong attenuation (Q<100), Hale method becomes highly unstable, so the next method in order of accuracy, i.e. nonstationary inverse-*Q* filter, is chosen instead.

Figures 6 to 8 show the results obtained for Q=100, when the Hale inverse-*Q* filter with *Q* values of 100, 150 and 80, is compared to the Gabor deconvolution. The phase

correction performed by Gabor deconvolution is very good; the lag is zero in the first half of the trace and around 1 ms. in the second half. The *Q* filter performs an almost perfect phase correction in the three cases. These results are consistent with the recommendation made by Duren and Trantham (1997) that is better to overestimate Q than underestimate it when applying *Q* filtering

Figures 9 and 10 show the results obtained for Q=50, when the Hale filter, using *Q* values of 50 and 56, is compared to the Gabor deconvolution . For Q=50 the correction of the inverse-*Q* filter is virtually perfect, but for Q=56 it turns unstable. The Hale inverse-*Q* method is substituted for the nonstationary inverse-*Q* method at this point. Figures 11 and 12 show the results when the nonstationary inverse-*Q* filter, with *Q* values of 56 and 65, is compared to the Gabor deconvolution. The Gabor deconvolution corrects the phase very well in the first two-thirds of the trace, but in the last third an important lag, reaching almost 4 ms, remains. When a *Q* value of 65 is used in the nonstationary inverse-*Q* filter, the phase correction of the two methods is similar.

Figures 13 to 15 show the same comparison for Q=20, when the nonstationary *Q* filter is applied with *Q* values of 20 and 22. The Gabor deconvolution seems to perform a very good job in this case, and the lag is around zero along the majority of the trace. However, something strange can be observed in the crosscorrelation plot: in several places, especially in the second half, the crosscorrelation coefficient is negative, though its absolute value is kept in the same order of magnitude. Enlarging a few events in different parts of the trace, Figure 14, it can be observed that the Gabor deconvolution apparently restores the correct position of the events but applies a phase rotation, in this case of approximately π, although the effect can be interpreted as a growing phase delay (which can be appreciated clearly in event 2) accompanied by a phase rotation.

DISCUSSION

The enlargement of a few events in the results obtained, Figures 3 and 14, indicate that the lag of MAXCORR can be accepted just approximately as a valid estimation of the phase correction, and that its reliability decreases when attenuation increases. According to this attribute, the phase correction performed by the Gabor deconvolution corrects only partially the phase-delay introduced by velocity dispersion but without reaching the phase-delay values corresponding to the difference between the analytical and the digital approach in the forward-modelling process. For Q equal to 100 (Figure 6 (f)), the remaining phase delay is less than a half of the difference between the analytical and the digital phase delay in forward-modelling, for the same Q value (Figure 3). For Q=50, the phase correction is practically perfect in the first two-thirds of the trace and then increases rapidly to reach approximately 4 ms. For Q=20, a phase delay can be observed clearly in event 2 (Figure 14), and a phase rotation in events 3, 4 and 5. It is not certain that the cause of the flaws mentioned in the previous paragraph lies entirely with the Hilbert transform computation. An important difference between the computation of the Hilbert transform in the forward and the inverse cases is the kind of function that is integrated. In the first case, it is the attenuation function, Equation (3), which is linear with respect to frequency. In the latter case, a function that is similar to the exponential attenuation function, Equation (9), which is expected to decay more rapidly with ω, has to be integrated.

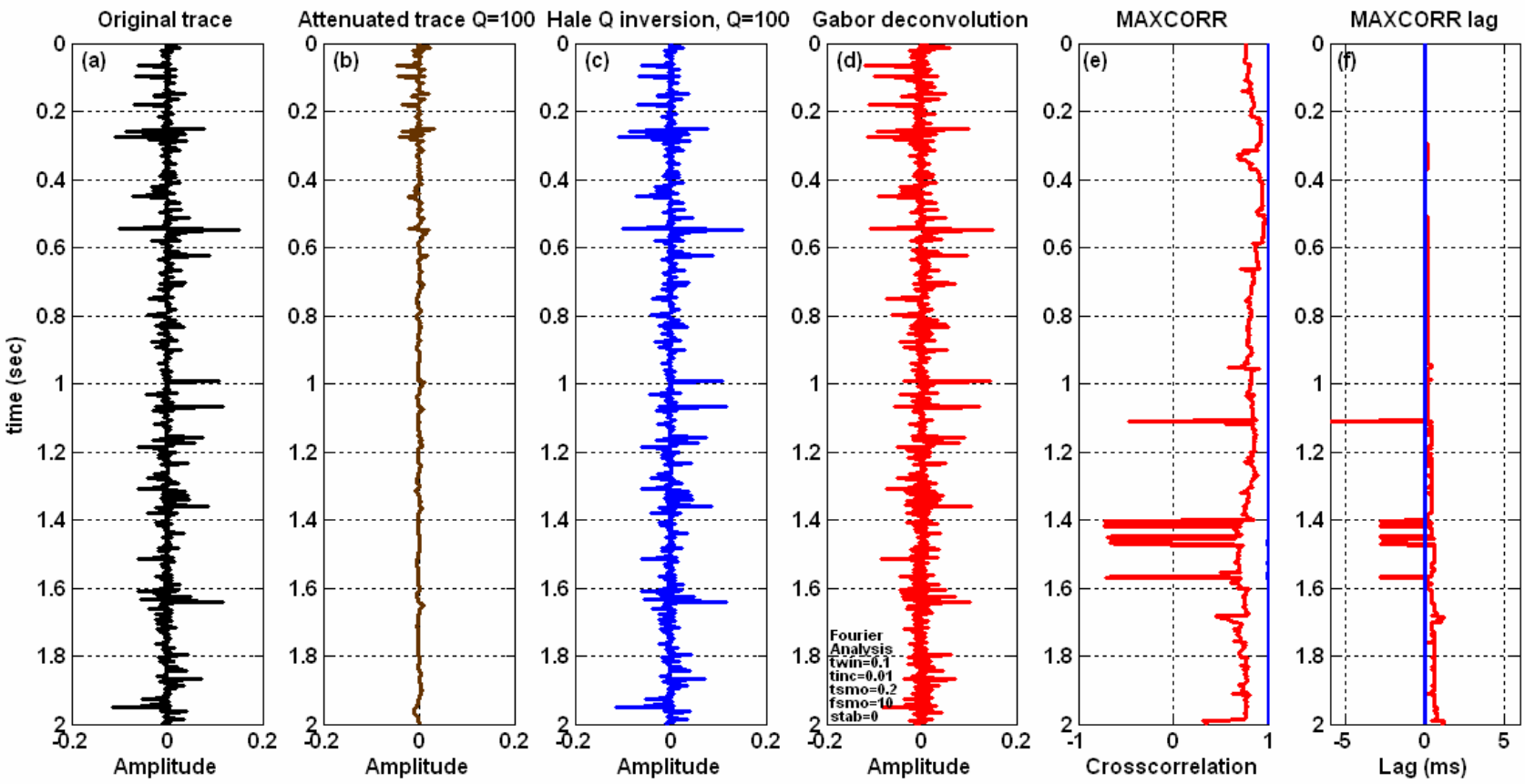

FIG. 6. Comparison of the results yielded by the Gabor deconvolution and the Hale inverse-*Q* filter by using the exact Q=100. Expected output (a) and attenuated input (b) traces are shown as references. The Hale inverse-*Q* filter (c) was applied with exactly the same *Q* value used to model (b). The results for the Gabor deconvolution (d) look very good, which is confirmed by the MAXCORR (e), approximately over 0.8, and its lag (f), approximately below 1 ms.

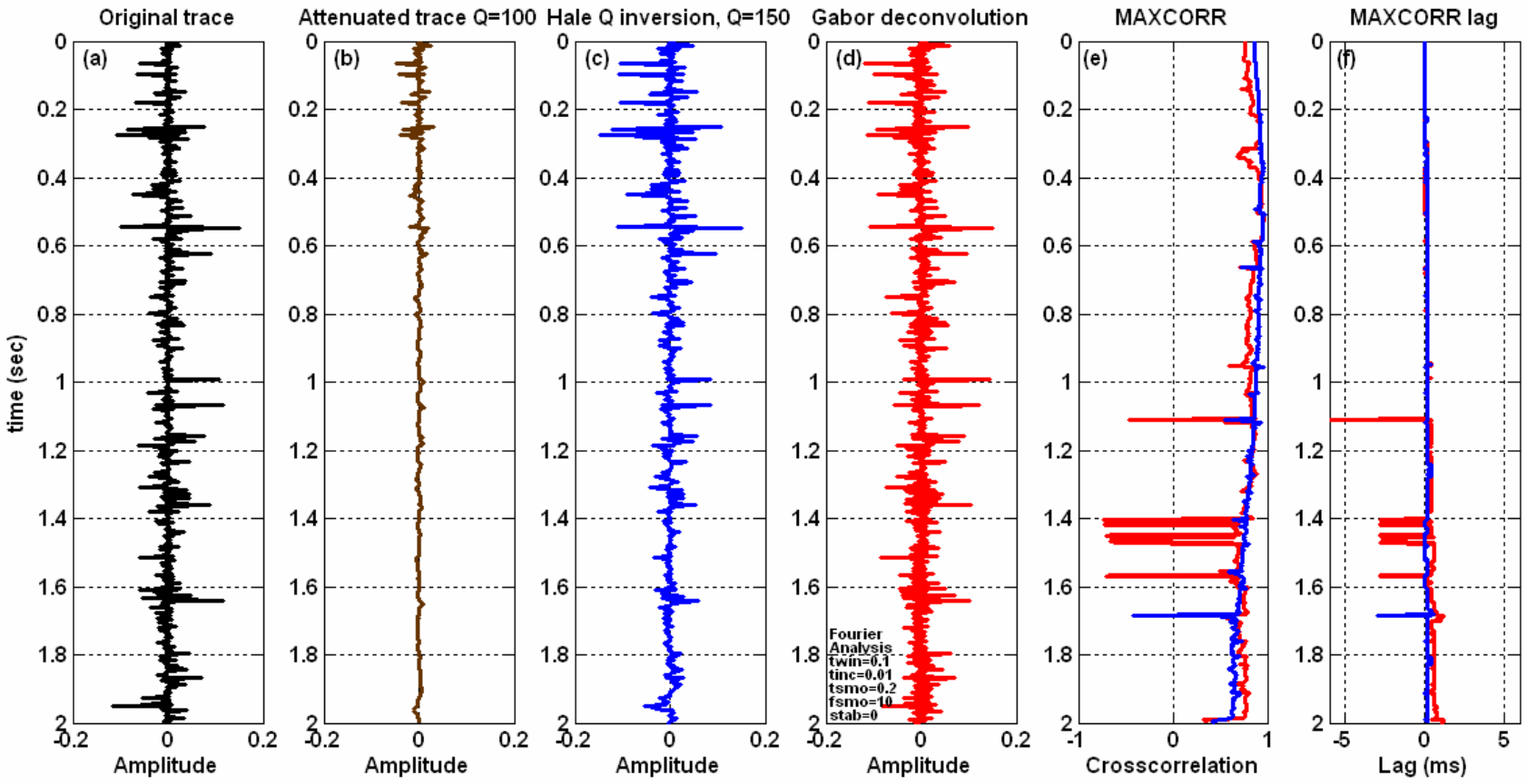

FIG. 7. Comparison of the results yielded by the Gabor deconvolution and the Hale inverse-*Q* filter by using an inexact *Q* (150) instead of the exact Q=100. Expected output (a) and attenuated input (b) traces are shown as references. The Hale inverse-*Q* filter (c) was applied with a *Q* value 50% greater than the one used to model the trace in (b). The results for the Gabor deconvolution (d) and the inverse-*Q* filter have approximately the same MAXCORR (e), but the MAXCORR lag for the Q filter (f) preserves its level of correction with respect to filtering using the exact Q value. The Inverse-*Q* filter is highly insensitive to *Q* overestimation for weak attenuation.

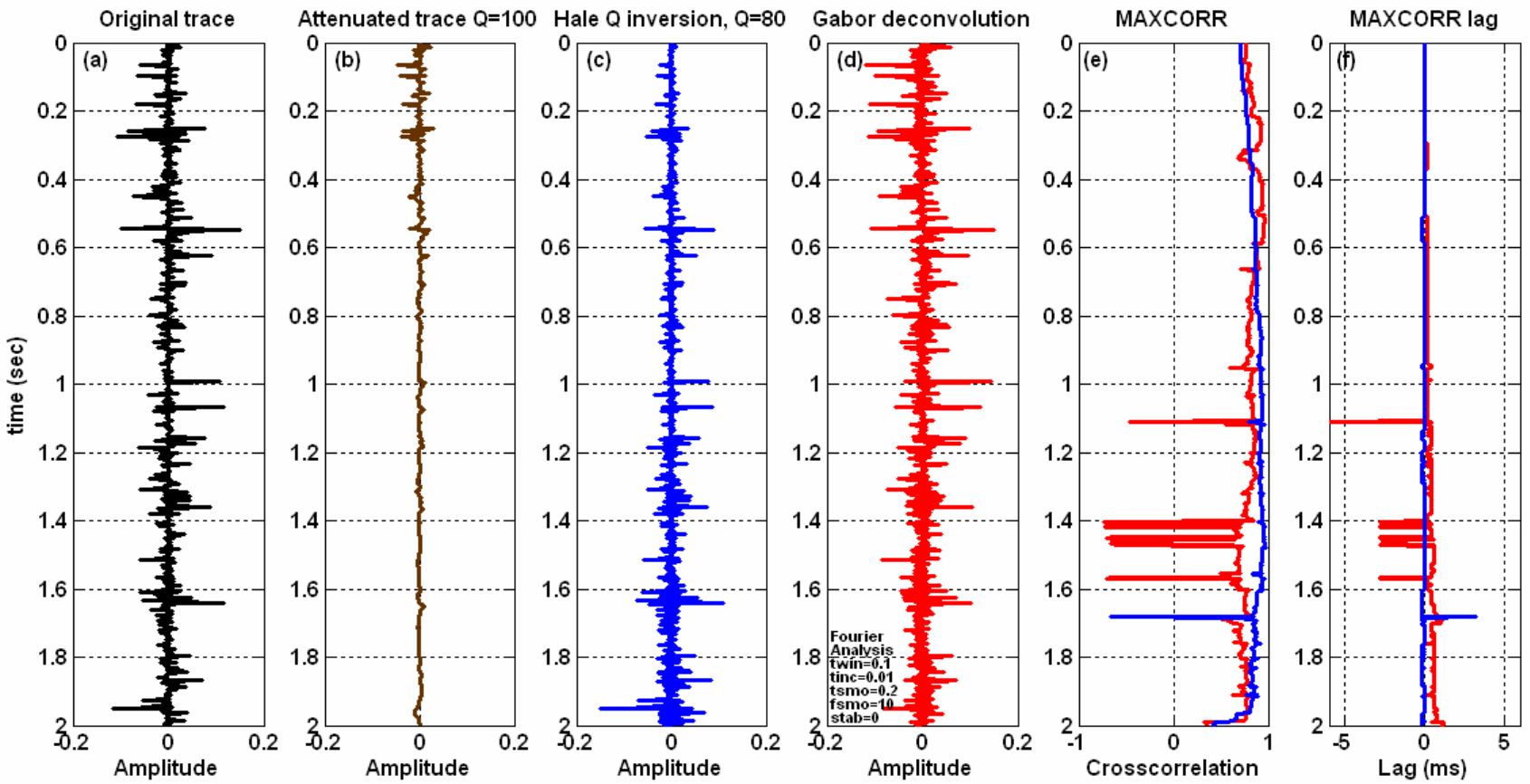

FIG. 8. Comparison of the results yielded by the Gabor deconvolution and the Hale inverse-*Q* filter by using an inexact *Q* (80) instead of the exact Q=100. Expected output (a) and attenuated input (b) traces are shown as references. The Hale inverse-*Q* filter (c) was applied with a *Q* value 20% less than the one used to model the trace in (b). Until this level of inaccuracy with respect to Q, the inverse-*Q* filter performs better, but instability problems start to arise for lower values of Q.

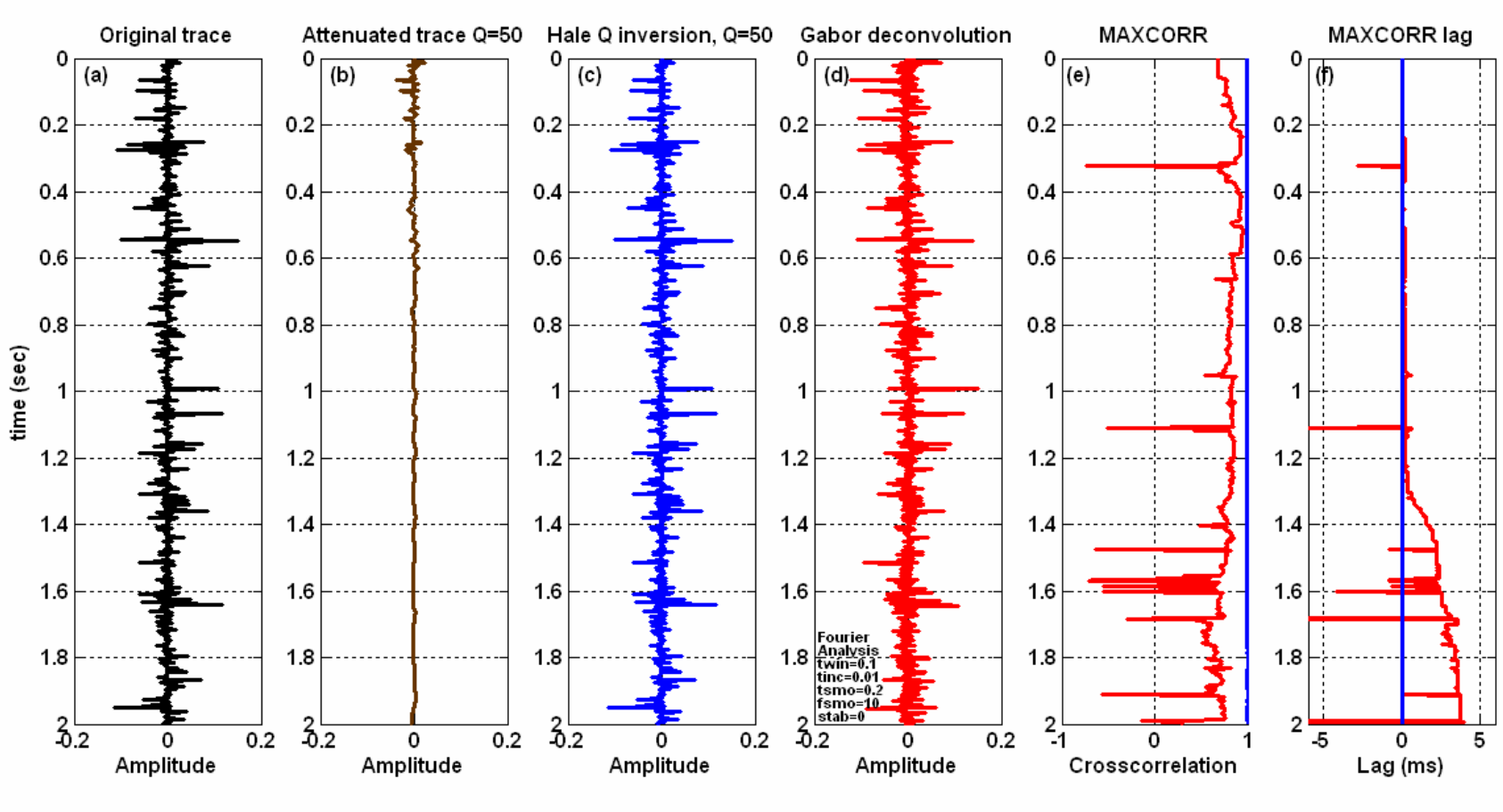

FIG. 9. Comparison of the results yielded by the Gabor deconvolution and the Hale inverse-*Q* filter by using the exact Q=50. Expected output (a) and attenuated input (b) traces are shown as references. The Hale inverse-*Q* filter (c) was applied with exactly the same *Q* (50) as the one used to model the trace in (b). The results for Gabor deconvolution are acceptable given the level of attenuation; the MAXCORR (e) has good values. The MAXCORR lag (f) shows appreciable values in the last third of the trace which indicates that an important phase delay remains in that part of the trace after Gabor deconvolution is applied.

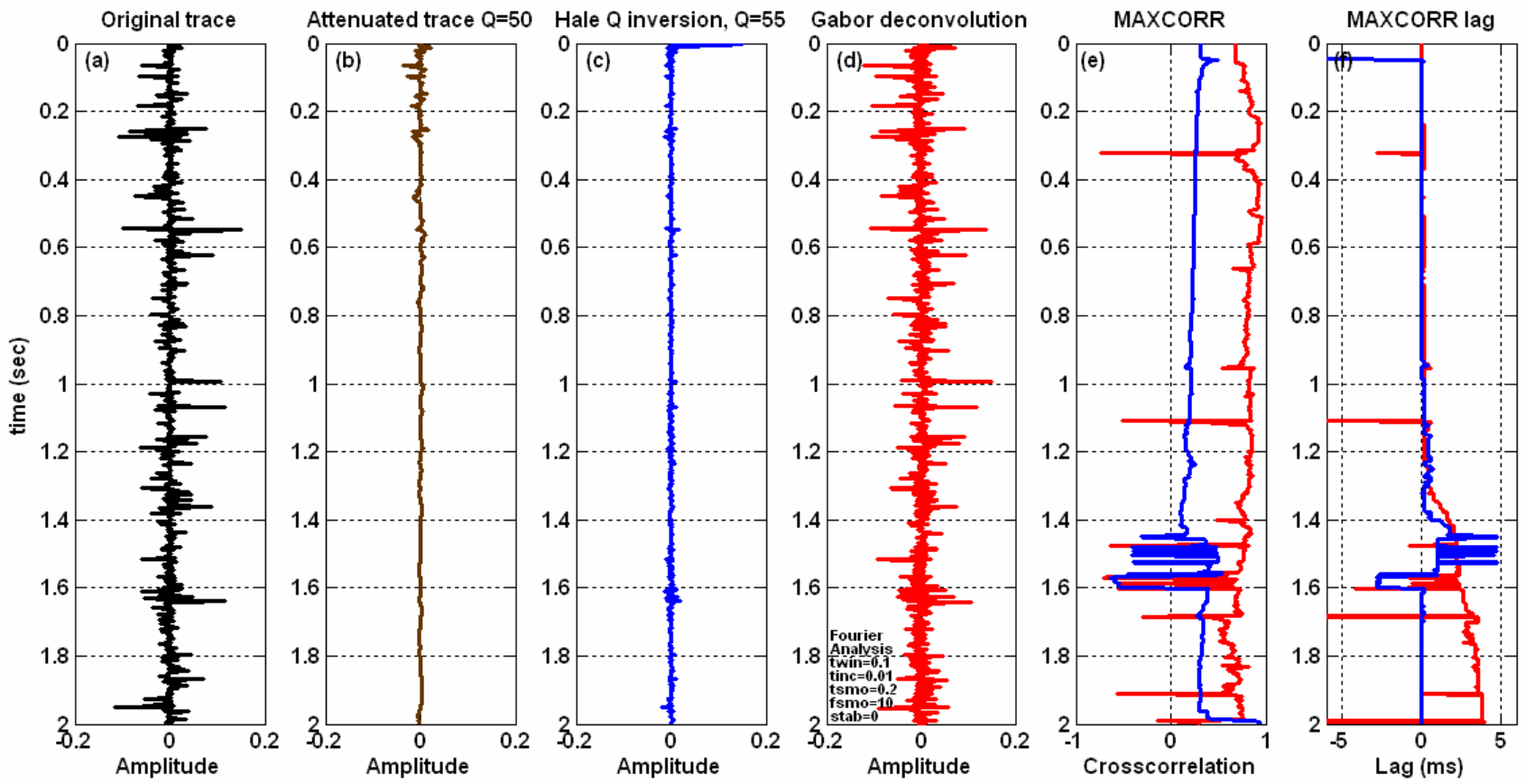

FIG. 10. Comparison of the results yielded by the Gabor deconvolution and the Hale inverse-*Q* filter by using an inexact *Q* (55) instead of the exact Q=50. Expected output (a) and attenuated input (b) traces are shown as references. The Hale inverse-*Q* filter (c) was applied with a *Q* value 10% greater than the one used to model the trace in (b); instability problems spoil the results.

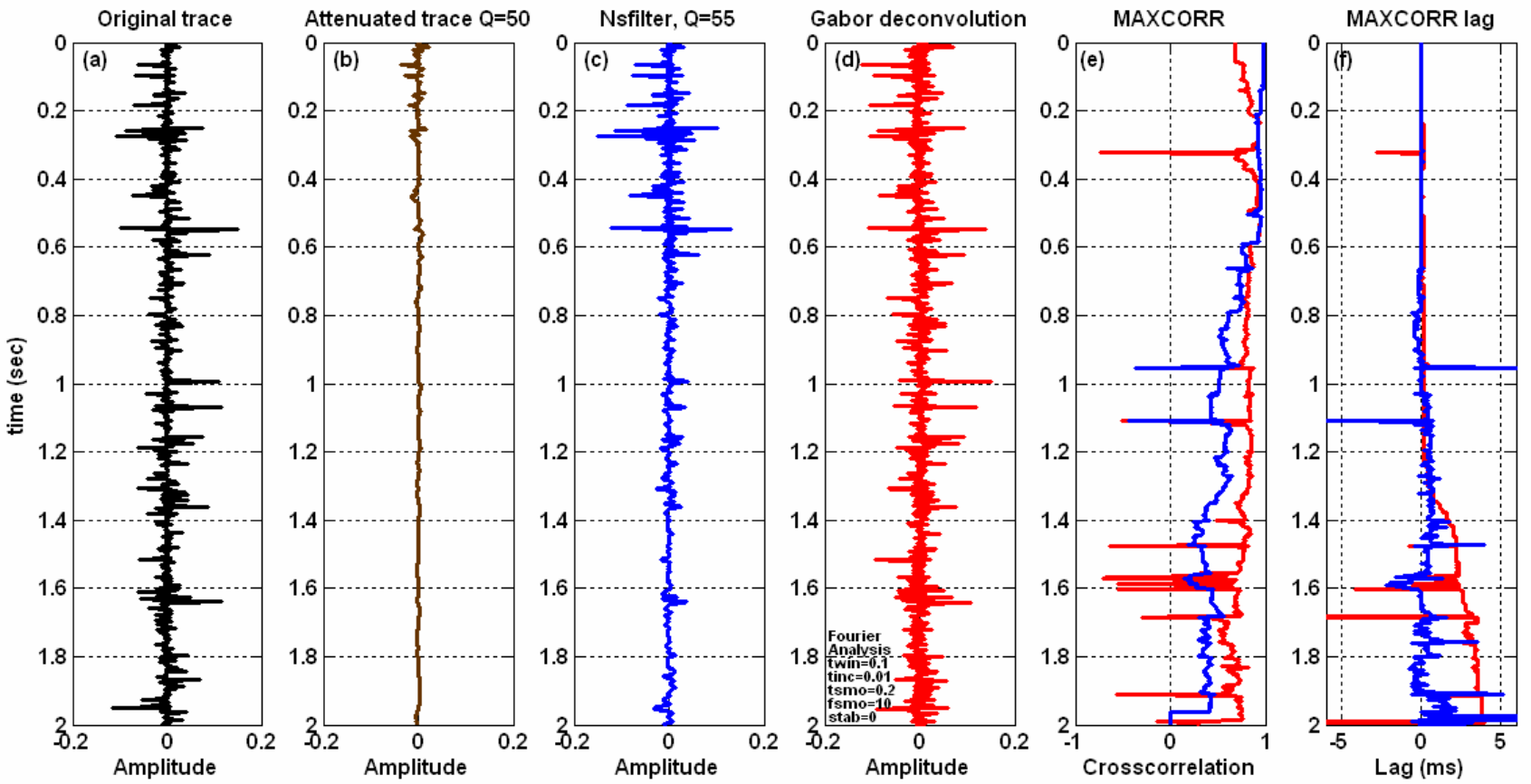

FIG. 11. Comparison of the results yielded by the Gabor deconvolution and the nonstationary inverse-*Q* filter by using an inexact *Q* (55) instead of the exact Q=50. Expected output (a) and attenuated input (b) traces are shown as references. The nonstationary inverse-*Q* filter (c) was applied with a *Q* value 10% greater than the one used to model the trace in (b). The Gabor deconvolution (d) has better MAXCORR (e) along the whole trace and similar MAXCORR lag (f) except in the last third of the trace.

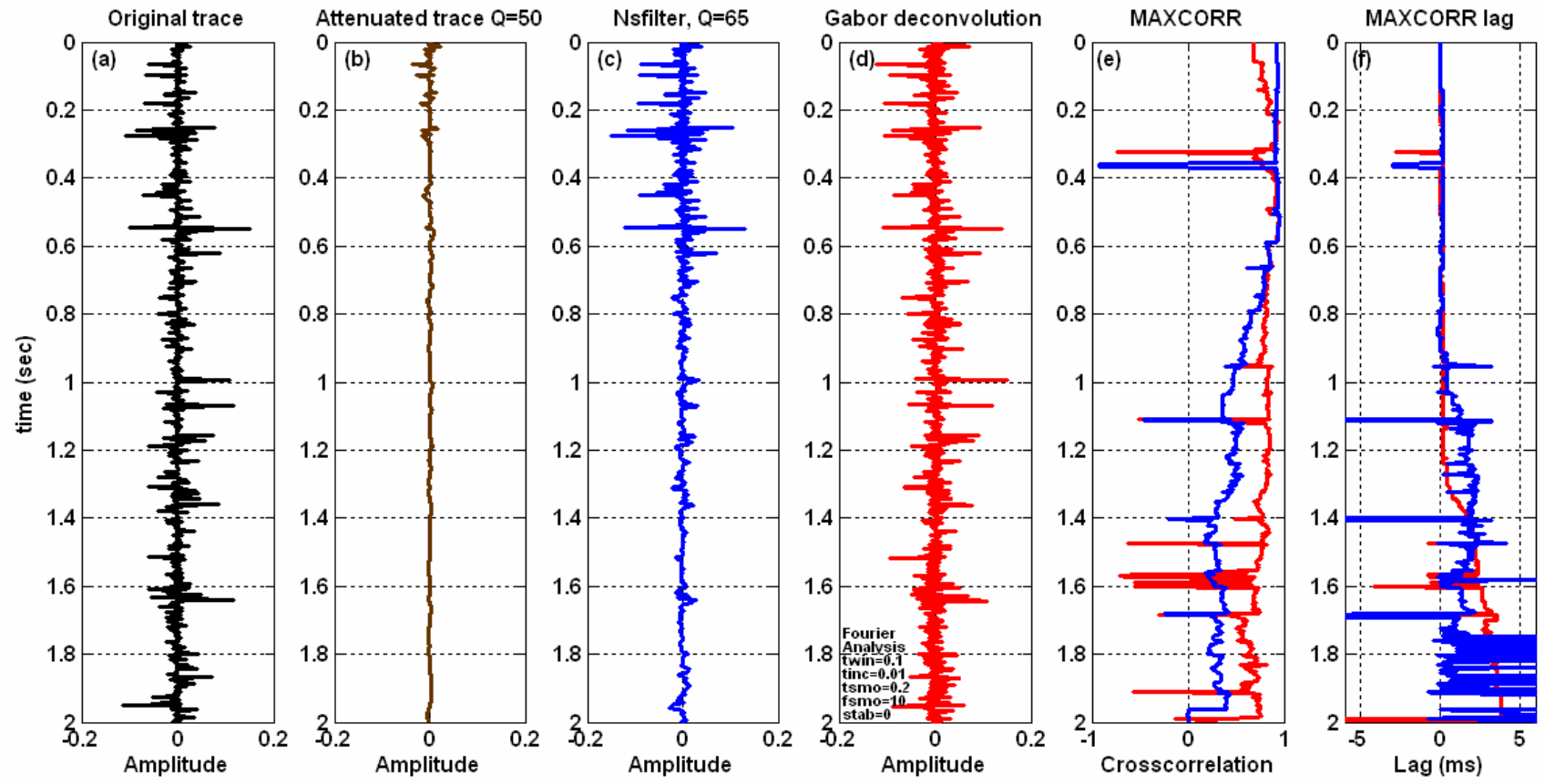

FIG. 12. Comparison of the results yielded by the Gabor deconvolution and the nonstationary inverse-*Q* filter by using an inexact *Q* (65) instead of the exact Q=50. Expected output (a) and attenuated input (b) traces are shown as references. The Hale inverse-*Q* filter (c) was applied with a *Q* value 30% greater than the one used to model the trace in (b). The Gabor deconvolution has better MAXCORR (e) and similar MAXCORR lag (f) along the whole trace.

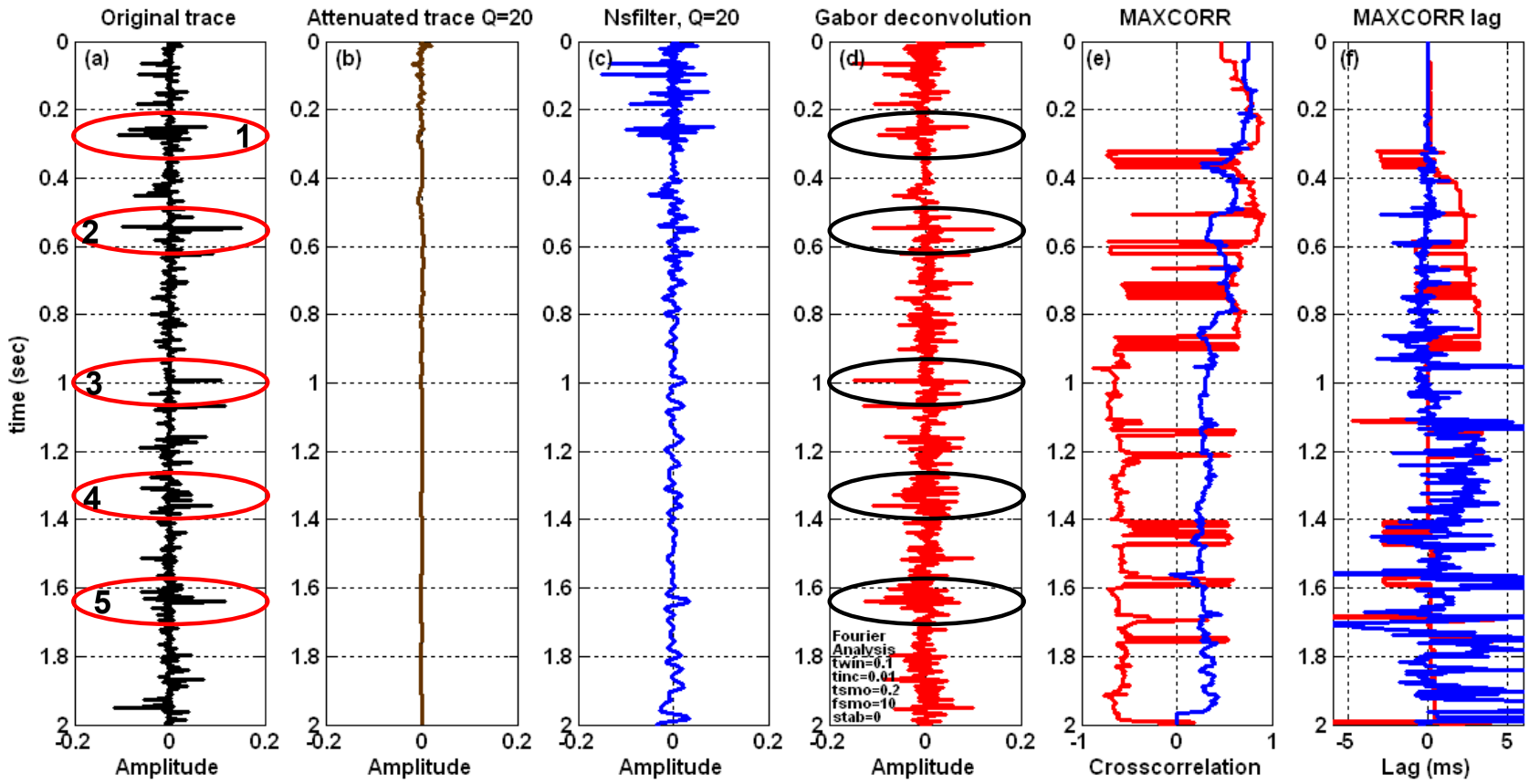

FIG. 13. Comparison of the results yielded by the Gabor deconvolution and the nonstationary inverse-*Q* filter by using the exact Q=20. Expected output (a) and input trace (b) are shown as references. The nonstationary inverse-*Q* filter (c) was applied with exactly the same *Q* (20) as the one used to model the trace in (b). The results for Gabor deconvolution are better both in MAXCORR (e) and in MAXCORR lag (f). It is remarkable that the crosscorrelation turns negative in the second half of the trace though keeping its absolute value, which indicates that a rotation in the phase is affecting that part of the trace. In Figure 14, the marked events are zoomed in to observe in more detail this effect.

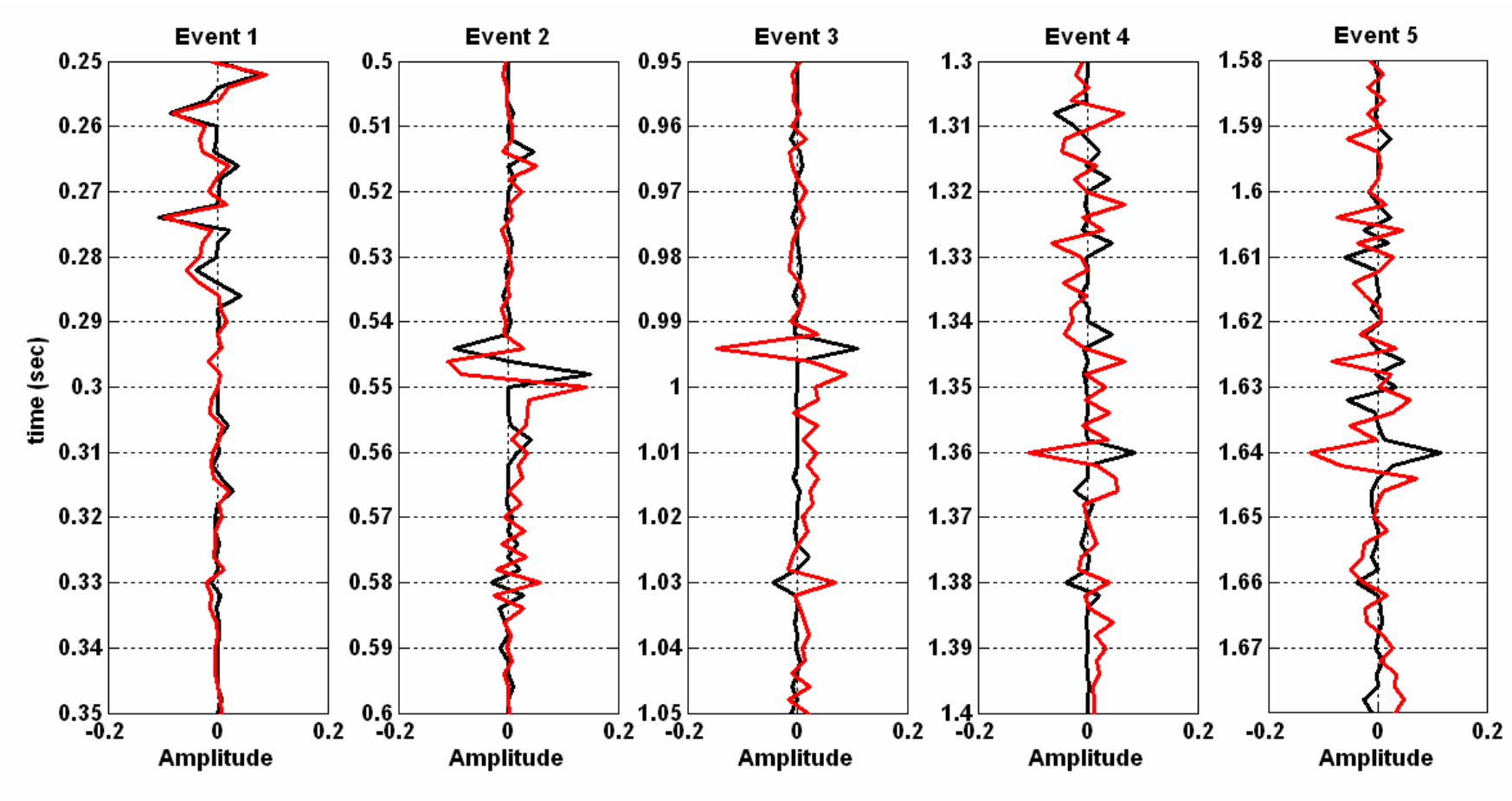

FIG. 14. A close-up of the events marked in Figure 13. The expected output and the Gabor deconvolution output are superimposed. In event 1 there is a good match between the two traces. In event 2 a phase delay is clearly observed. In figures 3, 4 and 5, a phase delay is accompanied by a phase rotation or a change in the waveform.

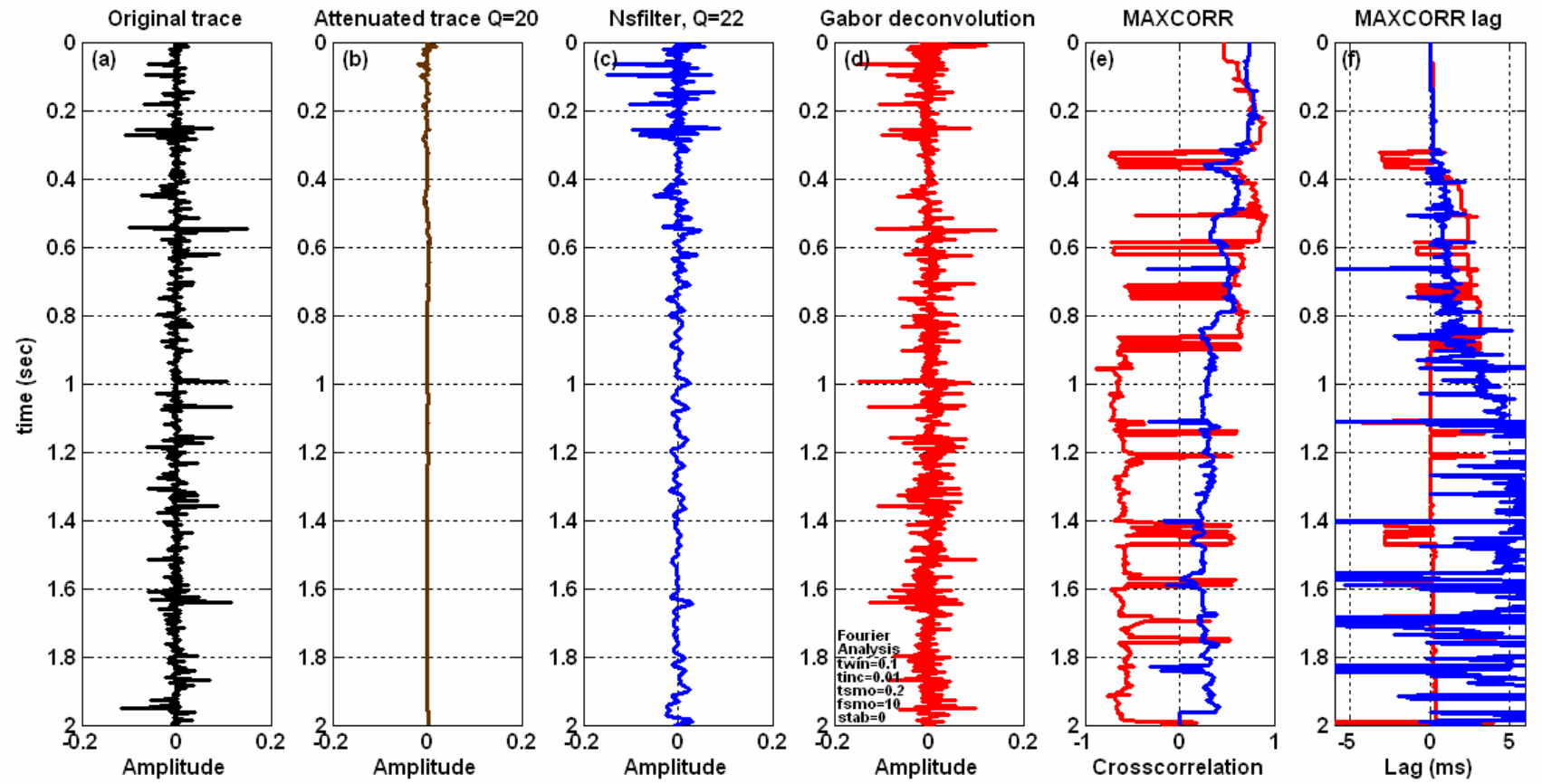

FIG. 15. Comparison of the results yielded by the Gabor deconvolution and the nonstationary inverse-*Q* filter by using an inexact *Q* (22) instead of the exact Q=20. Expected output (a) and attenuated input (b) traces are shown as references. The nonstationary inverse-*Q* filter (c) was applied with a *Q* value 10% greater than the one used to model the trace in (b). The Gabor deconvolution has better MAXCORR (e) and MAXCORR lag (f) along the whole trace.

Independent of the validity of the previous argument, the identified flaws in the phase correction by the Gabor deconvolution must be analyzed more carefully, the real cause established and a solution found.

A definitive judgment about the assessment considered in this work just can only be found by complementing the test done here with similar test using real surface seismic, VSP data and well logs.

CONCLUSIONS

Computation of the Hilbert transform for discrete functions can introduce an appreciable error thorough substituting the infinite limits in the integral for finite limits in the summation. This can be corroborated in the forward modelling of an attenuated trace according to the constant-Q theory. This theory provides an analytic way to compute the Hilbert transform, which can be used as reference for estimating the error committed by using a discrete approximation to the integral. The Gabor deconvolution is applied to attenuated traces and its phase-correction performance is compared with that obtained by using inverse-Q filtering methods. For weak attenuation (Q>100), inverse-Q filtering is highly insensitive to the uncertainty associated with the Q value. For this level of attenuation, the phase correction using Gabor deconvolution is very good, the remaining phase delay is within a half time sample although the Q filter performs better even when the Q used is 50% greater. For strong attenuation (Q<100), the performance of the Gabor deconvolution is better than the inverse-Q filter. When Q decreases, the inverse-Q filter results are increasingly sensitive to the uncertainty associated with Q and the Gabor deconvolution preserves the quality in its performance even for Q values as low as 20. As a result, the advantage in favour of the Gabor deconvolution increases when Q decreases. Given the fact that the Gabor deconvolution does not require any value of Q at all to yield results comparable to those obtained using any Q filtering method is an enormous difference in its favour.

A couple of flaws in the phase correction by Gabor deconvolution were observed: a comparatively large value for the remaining phase error (2 samples) in the last third of the trace for Q=50, and a rotation of the phase especially in the final half of the trace for Q=20. Neither problem seems to be part of a trend nor be caused by the discrete computation of the Hilbert transform involved in the Gabor deconvolution, but further research is needed to clarify and correct it.

FUTURE WORK

Consider models where Q changes with depth. Investigate and correct the causes of the flaws detected in correcting phase by Gabor deconvolution. Extend the tests to real data, using surface seismic data, VSPs and well logs. Improve the performance of the MAXCORR lag as phase-delay indicator.

ACKNOWLEDGEMENTS

The authors would like to thank the sponsors of the CREWES Project, the Canadian government funding agencies NSERC and MITACS, the CSEG and the University of

Calgary Department of Geology and Geophysics for their financial support to this project.

REFERENCES

Aki, K., and Richards, P. G., 2002, Quantitative Seismology: Theory and methods. University Science Books.

Dasgupta, R., and Clark, R. A., 1999, Estimation of *Q* from seismic surface reflected data: Geophysics, **63**, 2120-2128

Duren, R. E., and Trantham, E. C., 1997, Sensitivity of the dispersion correction to Q error: Geophysics, **62**, 288-290.

Gabor, D., 1946, Theory of communication: J. Inst. Electr. Eng., **93**, 429-457.

Grossman, J. P., Margrave G. F., Lamoureux M. P., and Aggarwala, R., 2002, Constant-*Q* wavelet estimation via a Gabor spectral model : CSEG Convention Expanded Abstracts.

Grossman, J. P., Margrave G. F., and Lamoureux M. P., 2002, Constructing nonuniform Gabor frames from partition of unity. CREWES Research Report, **14**

Kjartansson, E., 1979, Constant-*Q* wave propagation and attenuation: J. Geophysics. Res., **84**, 4737-4748

Hale, D., 1981, An Inverse-*Q* filter: SEP Report **26**.

Iliescu, V., and Margrave G. F., 2002, Reflectivity amplitude restoration in Gabor deconvolution: CSEG Convention Expanded Abstracts.

Iliescu, V., 2002, Seismic signal enhancement using time-frequency transforms. Thesis M.Sc. University of Calgary,

Margrave, G. F., 1998, Theory of nonstationary linear filtering in the Fourier domain with application to time-variant filtering: Geophysics, **63**, 244-259.

Margrave, G. F., and Lamoureux M. P. 2002, Gabor deconvolution: 2002 CSEG Annual Convention, Calgary, AB.

Margrave G. F., Dong, L. Gibson, P., Grossman, J. P., Henley D., and Lamoureux M. P., 2003, Gabor Deconvolution: Extending Wiener's Method to nonstationarity: CREWES Research Report, **15**.

Mertins, A., 1999, Signal Analysis: John Wiley and Sons.

Montana C. A., and Margrave G. F., 2004, Compensating for attenuation by inverse-*Q* filtering, CREWES Research Report, **16**.

Schoepp, A. R., and Margrave, G. F., 1998, Improving seismic resolution with nonstationary deconvolution: 68th Annual SEG meeting.

Schoepp, A. R., 1998, Improving seismic resolution with nonstationary deconvolution. Thesis M.Sc. University of Calgary

Wang, Y., 2002, An stable and efficient approach of inverse-*Q* filtering: Geophysics, **67**, 657-663.